

Shortcomings of classical phenological forcing models and a way to overcome them

Klaus Blümel*, Frank-M. Chmielewski

Agricultural Climatology, Faculty of Agriculture and Horticulture, Humboldt-University of Berlin, Germany

ARTICLE INFO

Article history:

Received 13 January 2012

Received in revised form 19 April 2012

Accepted 1 May 2012

Keywords:

Phenological modelling
Spring-Warming model
Beginning of blossom
Photoperiod
Climate change
Model comparison

ABSTRACT

A theoretical study proves that the common Spring-Warming model, which is widely used in phenological studies and frequently described in the literature, has systematic defects that do not allow a reliable projection of phenological stages for the future (e.g., up to 2100). When calculating spring phenological phases (e.g., beginning of blossom or leaf unfolding, etc.), defects occur because either the advance in blossom is included implicitly in the model and cannot be calibrated sufficiently to observations, or the model parameters attain unphysiological values or lie in a range so that a prognosis for the far future cannot be accomplished. Therefore, the introduction of a daylength term is suggested, which improves the Spring-Warming model and eliminates almost all of the discussed shortcomings. The performance of this improved model is demonstrated by calculating the beginning of apple blossom in Germany. For this purpose, we compared the improved model (M1) with three different versions of the original Spring-Warming model (M2–M4). The models were calibrated (optimized) using observed blossoming and temperature data (1962–2009), which have been regionalized on a 0.2° grid. The optimization was done for a representative grid point. The performance of the various model versions in predicting the beginning of apple blossom was compared with observations from independent years, which were not used in the optimization. Also, the beginning of blossom and its possible future changes were calculated with these models, using temperatures from the Regional Climate Model REMO-UBA with GHG emission scenario A1B (2001–2100). The new daylength term improved the performance of model M1 remarkably, and the model calibration automatically led to model parameters with meaningful values. These results, which were confirmed by other fruit tree species and locations, provided strong evidence that the conventional Spring-Warming models in phenology must be extended by photoperiodic sensitivity, at least for species which are photosensitive.

© 2012 Elsevier B.V. All rights reserved.

1. Introduction

Many people working in tree phenology (e.g., Chuine et al., 2010; Morin et al., 2009; Vitasse et al., 2011) have claimed that phenological phases in spring (beginning of leaf unfolding or blossom of most plant species, etc.) are predominantly controlled by the course of air temperature. In contrast, some authors (e.g., Körner and Basler, 2010) have suggested that because of photoperiodic constraints, observed effects of temperature on spring lifecycle events cannot be extrapolated to future temperature conditions on the basis of models driven by temperature alone. In the last few years there have been an increasing number of studies, which claimed

that photoperiod plays an important role in driving phenophases (Häkkinen et al., 1998; Schaber and Badeck, 2002; Körner, 2006; Linkosalo et al., 2006; García-Mozo et al., 2009a, 2009b). However, most stated that it is only important for mean- and late-flowering species and less essential for early-flowering fruits like peaches and apricots (Hunter and Lechowicz, 1992; Körner and Basler, 2011; Hänninen, 1995; Körner, 2006). An evaluation of 12 different phenological models for 11 North American woody species indicated support for the Spring-Warming models with photoperiod limitations (Migliavacca et al., 2012). There is still an on-going controversial discussion on this issue.

Much compelling evidence demonstrates photoperiodism working as a mechanism to prevent plants from a too-early break of ecodormancy and constrains the influence of temperature on development to 'safe periods', i.e., far away from frost damage. Apple and pear are examples of species that are not temperature-only driven (Körner, 2006). Körner stated that photoperiodism protects them from premature bud break. This statement is

* Corresponding author at: Humboldt-University of Berlin, Faculty of Agriculture and Horticulture, Professorship of Agricultural Climatology, Albrecht-Thaer-Weg 5, 14195 Berlin, Germany. Tel.: +49 30 31471222; fax: +49 30 31471211.

E-mail address: Klaus.Blumel@agrar.hu-berlin.de (K. Blümel).

contrary to what Heide and Prestrud (2005) claimed. They argued that apple and pear trees are not influenced by daylength, but only by temperature.

Physiologically, Körner and Basler (2010) argued that a lack of sufficient chilling in mild winters may delay bud break but may also be partially replaced by longer photoperiods. This hypothesis is confirmed by experiments performed by Caffarra and Donnelly (2011), but seems to depend on the species under consideration. This means that photoperiodic mechanisms in plants are not only an insurance against a too-late induction of dormancy, but also against a too-early “dormancy” break in the season (Körner, 2006) and against too-early and too-late blossom. An attempt to incorporate photoperiodism as a covariate to temperature in phenological models was made by Schaber and Badeck (2003) in a promoter-inhibitor model (PIM). This approach differs widely from ours. The PIM resulted in a better fit and validation relative to the classical model (i.e., without photoperiodism). However, these improvements could not be confirmed by Linkosalo et al. (2008), because an external validation, calculated using independently estimated model parameters, resulted in much higher external root mean square errors than for the other, simpler models, which were also tested in their study. They argued that this poor performance was caused by over-parameterization because the PIM has a total of 10 parameters.

Our own numerical computations for this study using the common, temperature-only driven phenological models for apple led to the following results: Calibration of the model parameters often resulted in more or less meaningless values. For example, the starting date of temperature accumulation t_1 [see Section 2.1, Eq. (1)] attains very late values and falls on dates when the temperature forcing has already begun or, at least, will have begun in the far future due to climate warming. That is exactly the criticism made by Linkosalo et al. (2008) of the Unified and Spring-Warming model.

Optimizing the model parameters in the period 1961–2009 with t_1 held constant at meaningful, small values, leads to a model which is unable to predict any prescribed trend for the beginning of blossom, especially if the forecast range is long and extended up to the year 2100. The model has its own built-in trend and cannot be calibrated to calculate any trend which differs significantly from this built-in trend. Furthermore, this model shows substantial systematic error (Fig. 9) and the base temperature T_{BF} [Eq. (2)] becomes much too low to have any physiological meaning. [Heat stimuli are only accumulated if the daily mean air temperature is greater than T_{BF} (see Eq. (3) and (4)).] Additionally, the forcing requirement F^* and T_{BF} are strongly interdependent and thus their parameter values are partly exchangeable (increasing F^* and decreasing T_{BF} and vice versa), which causes very large confidence intervals for these two parameters (see Section 4, Fig. 8).

In the first theoretical part of this paper (Section 2.2), we will use analytical integration to prove why the typical, commonly used Spring-Warming model has the undesirable properties mentioned above.

Then we will proceed finding a way to overcome these shortcomings (Section 2.3). Linkosalo et al. (2006) argued that, besides chilling and forcing, other environmental factors such as changes in light conditions are involved in the regulation of the timing of budburst. We will show that their question “Is there something missing?” seems to have the answer “yes”. For this purpose we will include an additional quantity (*daylength*) in the phenological model.

In the subsequent sections we will demonstrate, by comparing the performance of the old model versions (M2–M4) with the improved model (M1), that almost all deficiencies are eliminated and the forecast is essentially improved by this daylength term.

2. Scientific background

2.1. Forcing model for the beginning of blossom

In the present climate in Germany, dormancy of most fruit trees is released on average before the end of December (Chmielewski et al., submitted for publication). Thus, for now the plants can be assumed to be in the state of quiescence from the beginning of January, ready to react to favourable temperatures.

“Forcing” describes, very vaguely, the accumulation of heat stimuli for a plant following the period of dormancy. When sufficient heat portions are accumulated the plant will start flowering. A very well-known and widely used forcing model for the beginning of blossom of many plant species is the Spring-Warming model. It has the form

$$F^* = \sum_{i=t_1}^{t_2} R_f(T_i) \Delta t \quad (1)$$

$R_f(T_i)$ is a function of the daily mean temperature T_i on day i and is called the forcing rate function. Δt is the time step, usually 1 day (1 d). The smallest summation index t_2 , for which the sum on the right side approaches or exceeds the prescribed plant-specific forcing requirement F^* is the date (day of year = DOY) of the beginning of blossom in the year under consideration. The starting day t_1 of the summation is prescribed as a fixed value (e.g., 1 January) or has to be determined by optimization. In a forcing model which is supposed to be a mechanistic model and not a pure fitting model, t_1 should lie before the first forcing days but after the “release of dormancy”. If one applies Eq. (1) to spring temperatures T_i of several, subsequent years, one obtains a prediction for the beginning of blossom $t_2(pred, j)$ for each year j .

In the original version of the Spring-Warming model (Hunter and Lechowicz, 1992), the forcing rate function according to Eq. (2) is used:

$$R_f(T_i) = \max(T_i - T_{BF}, 0). \quad (2)$$

The summation in (1) [with (2) inserted for $R_f(T_i)$] is made up of the difference between the daily mean temperature T_i on day i and a plant-specific base temperature T_{BF} , provided that this difference is greater than zero. If one uses (2) as forcing function in (1), the unit of F^* is K d. Phenologists denote this as growing degree days (GDD).

2.2. Shortcomings of the model (theoretical considerations)

The Spring-Warming model [Eq. (1) and (2)] can be approximated by an integral:

$$F^* = \int_{t=t_1}^{t_2} \max(T - T_{BF}, 0) dt. \quad (3)$$

The following computations can be performed for almost any arbitrary forcing functions. For this reason, $T - T_{BF}$ is replaced by an almost freely chosen function $f(x)$:

$$F^* = \int_{t=t_1}^{t_2} \max(f(T - T_{BF}), 0) dt \quad (4)$$

t is the time, now considered as a steady, continuous variable, measured in DOY. $f(x)$ is supposed to be a monotonous function of x and we assume that $f(T - T_{BF}) \leq 0$ if and only if $T \leq T_{BF}$ or $T - T_{BF} \leq 0$, respectively. In this case, the integrand in (4) is always zero if $T - T_{BF} \leq 0$.

Now we assume an idealized, linear increase of the temperature with time t in spring:

$$T(t) = at + b. \quad (5)$$

In this case, the integrand in (4) is zero, if and only if

$$at + b - T_{BF} \leq 0 \quad \text{or} \quad t \leq \frac{T_{BF} - b}{a} =: t_s, \quad (6)$$

respectively. The new quantity t_s , defined in (6), is the day of year when the forcing accumulation starts, provided the idealized linear temperature increase is valid. a and b are constants which should be determined in a way that the ‘slope a of temperature in spring’ and the ‘temperature level b of the year under consideration’ is reproduced as well as possible.

As long as $t_1 \leq t_s$ applies, t_s can be inserted as lower boundary of the integral in Eq. (4). In this case, one can omit the max-function, since now $f(T - T_{BF})$ is always positive. Now instead of (4) we can write

$$F^* = \int_{t=(T_{BF}-b)/a=t_s}^{t_2} f(T - T_{BF}) dt. \quad (7)$$

With the coordinate transformation

$$z := T - T_{BF} = at + b - T_{BF} \quad (8)$$

one gets for the lower and upper boundary of the integral

$$z_1 = at_s + b - T_{BF} = a \frac{T_{BF} - b}{a} + b - T_{BF} = 0 \quad (9)$$

and

$$z_2 = at_2 + b - T_{BF} \quad (10)$$

And from (8), it follows that

$$dt = \frac{dz}{a} \quad (11)$$

Thus (7) can be rewritten as

$$\begin{aligned} F^* &= \int_{z=0}^{at_2+b-T_{BF}} \frac{f(z)}{a} dz = \frac{1}{a} [F(at_2 + b - T_{BF}) - F(0)] \\ &= \frac{1}{a} g(at_2 + b - T_{BF}). \end{aligned} \quad (12)$$

$F(x)$ is the antiderivative of $f(z)$ and does not need any precise specification. $g(x)$ was inserted as a substitute for the term in brackets. It is important that the function $g(x)$ depends, as well as the term in brackets, only on the argument $at_2 + b - T_{BF}$. If $g(x)$ is invertible, one gets from (12)

$$at_2 + b - T_{BF} = g^{-1}(aF^*) \quad (13)$$

or

$$t_2 = \left[\frac{g^{-1}(aF^*)}{a} + \frac{T_{BF}}{a} \right] - \left(\frac{1}{a} \right) b \quad (14)$$

respectively. Eq. (14) is only correct as long as $t_1 < t_s = (T_{BF} - b)/a$ applies. Note that solution (14) no longer depends on t_1 . [$g(x)$ is invertible if $f(z)$ attains only positive or only negative values in the integral range. This is the case according to the suppositions; thus $F(z)$ is strictly monotone increasing or decreasing and hence invertible.]

Assuming that the slope a of the temperature course in spring is constant every year, and that the temperature level b varies from year to year, we can deduce from (14) that the “trend $\partial t_2 / \partial b$ of the date t_2 of beginning of blossom with reference to the temperature level b ” does not depend on either of the calibration parameters F^* and T_{BF} . These parameters only determine the value of the term in square brackets, which represents the offset in the linear t_2 - b relation. Because various tuples (F^*, T_{BF}) can generate the same offset constant, T_{BF} and F^* cannot be determined uniquely.

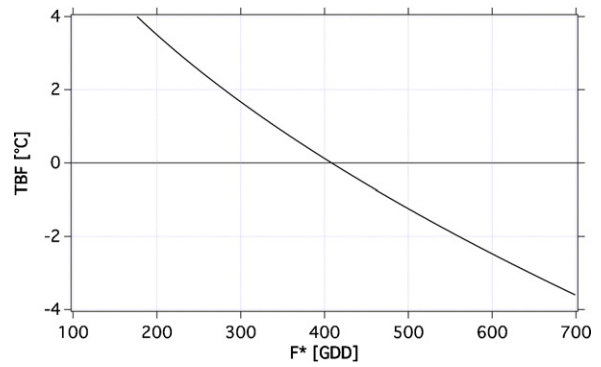


Fig. 1. Relation between T_{BF} and F^* in the indeterminate range of the Spring-Warming model (with $a=1/6 \text{ K d}^{-1}$ and $t_2(b=0^\circ\text{C})=70 \text{ DOY}$). Both parameters can attain all values on the curve without changing the model results as long as the relation $t_1 < t_s$ remains valid.

An analytical equivalent of Eq. (14) for the Spring-Warming model [Eq. (1) and (2)] follows if one inserts $f(z)=z$ into (12), performs the integration

$$F^* = \frac{1}{a} \frac{z_2^2}{2} = \frac{(at_2 + b - T_{BF})^2}{2a} = \frac{a(t_2 + (b/a) - (T_{BF}/a))^2}{2} \quad (15)$$

and solves (15) for t_2 :

$$t_2 = \left[\left(\frac{2F^*}{a} \right)^{1/2} + \frac{T_{BF}}{a} \right] - \left(\frac{1}{a} \right) b. \quad (16)$$

Formally, there are two solutions. A minus sign in front of $(2F^*/a)^{1/2}$ in (16) would also be a solution of (15). Since we want $t_2 > t_s$, the solution with the plus sign must be picked.

As long as $t_1 < t_s = (T_{BF} - b)/a$ is true, the term in square brackets can be held at a constant value c , even if T_{BF} is altered. Equating c with the term in square brackets and solving for T_{BF} gives

$$T_{BF} = ac - (2F^*a)^{1/2} \quad (17)$$

The indeterminate range of T_{BF} and F^* , described by (17), is shown in Fig. 1. For this figure, we have chosen $T_{BF} = 4^\circ\text{C}$, $b = 0^\circ\text{C}$, $a = 1/6 \text{ K d}^{-1}$ and $t_2 = 70 \text{ DOY}$ and calculated F^* from (15). Then c , which equals the square bracketed term in (16), could be derived. With c held constant on this value, F^* was varied and T_{BF} was calculated from (17).

The course of t_2 as a function of b and the trend $\partial t_2 / \partial b$, defined by (16), remains constant for every tuple (F^*, T_{BF}) on the line in Fig. 1, provided that t_1 , b and T_{BF} fulfil the condition $t_1 < t_s = (T_{BF} - b)/a$.

If we had observations of t_2 and b for several years, we could perform a linear regression and determine the regression parameters α and β for the relation $t_2 = \beta + \alpha b$. In that case, we would calculate β (the offset) instead of the term in brackets in (16) and α (the slope) instead of $-(1/a)$ in (16) directly with the help of the “normal equations”. The huge difference compared with (16) is that the regression is able to adapt the slope α to the real phenological trend, but the Spring-Warming model is not able to adjust the slope since $-(1/a)$ does not depend on the calibration parameters F^* and T_{BF} but only on the slope a of the temperature increase in spring [see Eq. (5)]. Hence, the slope in the Spring-Warming model is not at all related to the plant-specific trend of the date of flowering. Not even a change of the forcing function $R_f(T)$ or $f(T - T_{BF})$, resp., can eliminate this problem which can be deduced easily from (14). The calibration of the Spring-Warming model is additionally complicated by the fact that F^* and T_{BF} are not uniquely determined as long as $t_1 < t_s$ applies.

Fig. 2 proves that the trend $\partial t_2 / \partial b$ does not depend on F^* and T_{BF} , as long as the condition $t_1 < t_s$ is fulfilled. The graphic shows the course of t_2 as a function of b for different sets of (F^*, T_{BF}) . The

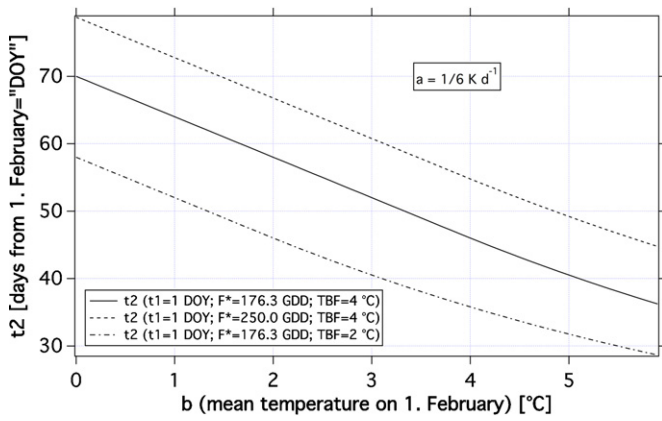


Fig. 2. Dependence of t_2 on the temperature level b in the Spring-Warming model at constant temperature increase “ a ” (linear with time) in spring (without day-to-day fluctuations) for different parameter sets (F^* , T_{BF}) with $t_1 = “1” = \text{const}$. The trend cannot be altered by changes in F^* and T_{BF1} .

slope is the same for all curves. Only for great b -values, when t_s becomes smaller than t_1 , the trend changes and becomes weaker. [b can be interpreted as the long-term average of air temperature on 1 February, since only after that date the increase of temperature in spring is approximately linear. Accepting this interpretation, t_1 and t_2 must be counted starting with 1 “DOY” on 1 February.]

Even for the case where the condition $t_1 < t_s$ is violated, an analytical solution for the Spring-Warming model can be specified. If $t_1 > t_s$ applies then

$$F^* = \int_{t=t_1}^{t_2} (at + b - T_{BF}) dt \quad (18)$$

has to be computed instead of (7) because now the integrand is already positive at t_1 . Integration leads to a quadratic equation for t_2 with solution

$$t_2 = t_s + \left[(t_1 - t_s)^2 + \frac{2F^*}{a} \right]^{1/2} \quad \text{for } t_1 > t_s$$

$$t_2 = t_s + \left[\frac{2F^*}{a} \right]^{1/2} \quad \text{for } t_1 \leq t_s \quad (19)$$

with $t_s := \frac{T_{BF} - b}{a}$ and $T(t) = at + b$.

Keep in mind that t_s is a function of b and T_{BF} for fixed a . Thus t_s is not constant if T_{BF} or b are varied. The second line of (19) matches (16) and is repeated here only for completeness. If $t_1 > t_s$, the trend $\partial t_2 / \partial b$ is no longer independent of the calibration parameters T_{BF} and F^* . This can be seen if the expression for t_s is inserted into the first line of Eq. (19) and the partial derivative with respect to b is taken [Eq. (20)].

$$\frac{\partial t_2}{\partial b} = -\frac{1}{a} + \frac{1}{a} \frac{t_1 - t_s}{[(t_1 - t_s)^2 + (2F^*/a)]^{1/2}} \quad (\text{for } t_1 > t_s) \quad (20)$$

For $t_1 \leq t_s$, the second term in (20) must be omitted so one obtains the constant trend $-1/a$, which we have already seen in Eq. (16).

In Fig. 3 not only the tuples (F^* , T_{BF}) are varied, but also t_1 . To obtain values comparable with the real Spring-Warming model, we have chosen $a = 1/6 \text{ K d}^{-1}$ for the temperature increase in spring again. This corresponds to a “trend of t_2 ” with -6 d K^{-1} provided that $t_1 < t_s$. F^* was chosen in a way that all curves have the same t_2 at $b = 0^\circ\text{C}$.

Because there are daily variations and the course of temperature is not exactly linear but rather matches a sine curve over the year, the idealized model (20) will show deviations compared with the real Spring-Warming model which is driven by observed

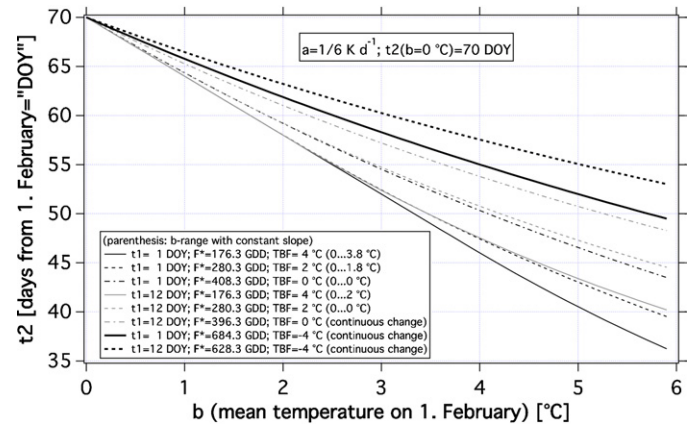


Fig. 3. Dependence of t_2 from temperature level b in the Spring-Warming model at constant temperature increase “ a ” (linear with time) in spring (without day-to-day fluctuations) for different parameter sets (t_1 , F^* , T_{BF}). The textbox shows (in parenthesis) the range for b with constant slope $\partial t_2 / \partial b = -1/a = -6 \text{ d K}^{-1}$ [the range follows from the condition $t_1 < t_s$ and t_s according to Eq. (6)].

temperatures. Nevertheless, the analytical model explains many of the unusual or unwanted properties of the true Spring-Warming model (as well as of related forcing models): The smaller T_{BF} and the greater t_1 , the less intense is the advance of t_2 for high values of b . High t_1 -values also achieve the reduction of the high negative trends already at relatively small b -values.

Direct integration of (18) leads to

$$F^* = \frac{1}{2} a (t_2^2 - t_1^2) + (b - T_{BF})(t_2 - t_1) \quad (\text{for } t_1 > t_s) \quad (21)$$

and from the second line of (19), by solving for F^* one gets:

$$F^* = \frac{a}{2} (t_2 - t_s)^2 \quad (\text{for } t_1 \leq t_s) \quad (22)$$

If one postulates that the average beginning t_2 of blossom always falls on the 70 DOY in the present climate at today’s temperature level $b = 0^\circ\text{C}$, and once again $a = 1/6 \text{ K d}^{-1}$, Eqs. (20)–(22) give the (today’s) trends $\partial t_2 / \partial b$ as a function of T_{BF} which are shown in Fig. 4.

Fig. 4 shows that: the greater t_1 and the smaller T_{BF} , the less negative is the trend of t_2 with b . This agrees with the results from Fig. 3. At $t_1 = 0 \text{ DOY}$ (solid black line), the trend remains constant at -6 d K^{-1} for all $T_{BF} > 0^\circ\text{C}$. At $t_1 = 12 \text{ DOY}$ (black dash-dotted line), the trend remains constant for all $T_{BF} > 2^\circ\text{C}$, etc. This means the model can be adapted to an observed trend (provided this observed trend is smaller in absolute value than -6 d K^{-1}) only if T_{BF} is unphysiologically small or the t_1 chosen is much greater than t_s . If the last condition applies, one runs into the danger that the starting date t_1 of temperature summation falls after the beginning of the real

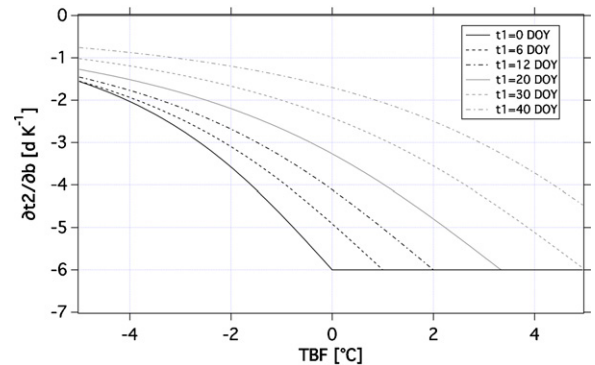


Fig. 4. Trend $\partial t_2 / \partial b$ as a function of T_{BF} at $b = 0^\circ\text{C}$ for different values of t_1 . F^* has been chosen in a way that $t_2(b = 0^\circ\text{C}) = 70 \text{ DOY}$ (with $a = 1/6 \text{ K d}^{-1}$). The start of the real forcing is at $t = t_s = 6(T_{BF} - 0^\circ\text{C}) \text{ d K}^{-1} = 6T_{BF}(\text{ }^\circ\text{C})^{-1} \text{ DOY}$ in this case.

forcing. In the idealized version with the linear temperature increase, presented here, there is not only a risk, but it is a fact that t_1 starts too late since t_s is the start of the actual forcing!

2.2.1. Summary of the preceding result

The trend $\partial t_2 / \partial b$ in the Spring-Warming model, and in all forcing models whose forcing function $R_f(T)$ fulfils the requirements mentioned at Eq. (4), does not depend on the calibration parameters T_{BF} and F^* , but only on the slope a of the temperature increase in spring (which is assumed to be constant in this study). This is true, as long as the start of the summation t_1 [see Eq. (1)] precedes the start t_s of the real forcing and as long as the smoothed course of the daily mean temperatures can be treated as approximately linear. However, if $t_1 > t_s$, the calibration parameters affect the trend. Namely, the effect is larger, the greater the t_1 and the smaller the T_{BF} selected.

With increasing b (increasing temperatures in the context of climate change), t_s becomes smaller [Eq. (6)]. As a consequence, the trend of t_2 , which is only determined by a in the present climate (provided that t_1 precedes the real start t_s of forcing and T_{BF} has a physiological meaningful value), will change in the future because t_s will become smaller than t_1 if a certain temperature level b is reached. The intensity of this change is defined by T_{BF} and F^* [Eq. (20)]. Both parameters cannot be calibrated properly for the current climate conditions because there is an indeterminate range (see Fig. 1) in which one parameter can be varied without changing the model results significantly. If t_1 is set to very small values, so that even in the far future the condition $t_1 < t_s$ remains valid, then, in general, the performance of the model is very poor for the present climate (i.e., large root mean square errors when validated with independent data). The trend is also much too negative, causing a too-large advance of the date of flowering. If very late t_1 -values are chosen, then the model can be calibrated much more precisely. But in this case, there is a risk of missing parts of the forcing period. The forcing requirement F^* could therefore be already partially fulfilled before accumulation in the model starts at t_1 in the future.

All these deficiencies lead to the conclusion that the period in which the plant is able to react to environmental stimuli, is described insufficiently by the conventional forcing models. Something is missing that prevents the plants from reacting too early to temperature stimulation.

2.3. A new approach to improve the Spring-Warming model

To improve the performance of the model, the forcing function $R_f(T)$ [Eq. (2)] was modified, supplemented and tested with additional quantities (sunshine duration, daily mean global radiation, mean global radiation over the daylength period, daylength itself, etc.). The best result for all tested quantities and fruit species, which we investigated up to now (apple, sour cherry, sweet cherry, pear, strawberry, grapevine, peach, apricot, plum), was found with the power function approach (23) instead of (2):

$$R_f(T) = \max(0., T - T_{BF}) \left(\frac{\text{daylength}}{10 \text{ h}} \right)^{EXPO} \quad (23)$$

Here *daylength* is the time between sunrise and sunset in hours. It depends on the day of the year and the geographical latitude and was calculated using the formulas from Muneer (2004). The “10 h” in the denominator is for normalization and to adjust the magnitude of F^* to values similar to the one used in the original Spring-Warming model. [Even though the magnitudes of (23) and (2) are similar, the forcing requirement F^* and the forcing rate function $R_f(T)$ of both models are not comparable because they represent different quantities. To emphasize that we will call the “unit” of F^* in the improved model PTU (instead of GDD) although the real physical units of both F^* are the same (K d).] *EXPO* is a new model

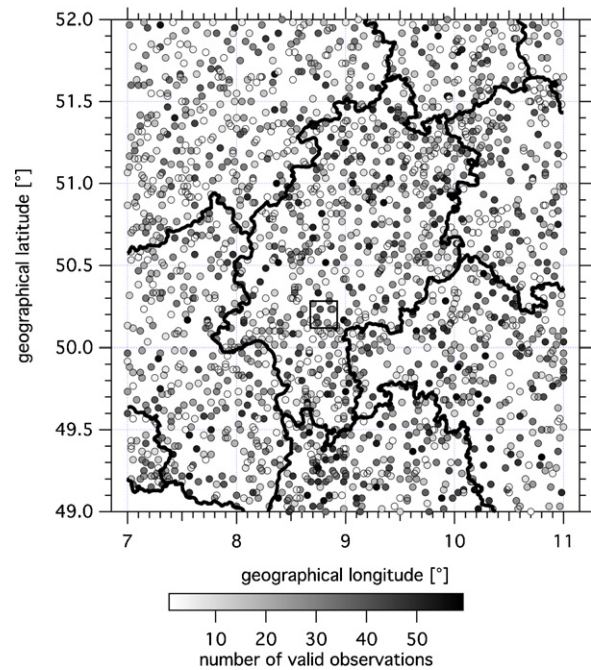


Fig. 5. Phenological stations with observations for the beginning of blossom of apple in the federal state of Hesse in Germany. Grey tones indicate the number of valid observations in the period 1951–2009. The small rectangle indicates the grid point near the city Frankfurt/Main.

parameter. Its value depends on the fruit species and on the region, and must be optimized in conjunction with the other parameters. Besides the simple power function dependency on *daylength* in the new factor in (23), we tested several different functions for this “DL-term”, including the four-parameter logistic equation (Motulsky and Christopoulos, 2003) with *Bottom* = 0, “*Top-Bottom*” = const. and optimized *LogEC50*- and *Hillslope*-parameters. But the simple factor in Eq. (23) showed the best performance.

Therefore, the next step in this study was to compare the performance of Eq. (23), called model M1 in the following, with three other models (M2–M4) which are based on the original Eq. (2).

3. Materials and methods

3.1. Phenological data

The decisive parameter for this study was the start of apple blossom (*Malus domestica*, early ripening variety with no further specifications). We analysed a total of 48 years of data for the beginning of apple blossom (BBCH 61) from 1962 to 2009. All available phenological data for Germany (between 800 and 3000 observations per year; Fig. 5 shows only a part of these phenological stations for the federal state of Hesse) were regionalized on a grid with 0.2° resolution (14 km × 22 km) and covered the whole area of Germany. This was done using second-order universal kriging (Wackernagel, 1998; Blümel and Chmielewski, 2011) with a drift term depending on height. The 81 grid points which cover the federal state of Hesse were then selected for our study. The model results will be discussed for a typical, individual grid point near Frankfurt/Main (8.8°E, 50.2°N, 149 m a.s.l.). This grid point is representative for all grid points in Hesse with intensive cultivation of apple trees, and it has a characteristic altitude and central location. In addition, we tested a “regional” model, which was designed to derive the best average results for all 81 grid points with a single parameter set. The results will not be shown here because they are very similar to the outcomes at the individual grid point.

3.2. Observed meteorological data

In order to model the annual date of beginning of apple blossom and to calibrate the models, we used air temperatures observed by the German Meteorological Service (DWD) from 1961 until 2009, which were provided within the research initiative INKLIM-A. These data were regionalized on a 0.2° grid using second-order universal kriging as with the phenological data. The grid also covers the state of Hessen with 81 grid points.

3.3. REMO-UBA data

In this study, only results from the dynamic regional climate model REMO-UBA will be shown (control run C20: 1971–2000 and GHG emission scenario A1B: 2001–2100). The results for models ECHAM5-CLM, HadCM3-CLM and WETTREG 2010 are qualitatively similar and not shown here.

REMO-UBA is a 3-dimensional, dynamic hydrostatic regional climate model with a spatial resolution of 0.088° (≈ 10 km) (Jacob et al., 2007). The sub-scale processes are calculated with the physical parameterizations of the global climate model ECHAM 4 (Roeckner et al., 1996). The global climate model ECHAM 5/MPI-OM (Roeckner et al., 2003) (spectral model with resolution T63; ≈ 200 km) is used to drive the regional model. The inner core model region of REMO-UBA includes Germany, Austria and Switzerland.

The temperature data from the regional climate scenarios were attributed to the same grid as the observed data.

All results of the Regional Climate Model (RCMs) were BIAS corrected on the $14 \text{ km} \times 22 \text{ km}$ grid since there are systematic departures between the control run of the model (C20) and the observation depending on the season and region. For temperature data (T) we used an additive model correction, which was based on monthly temperature deviations in the period 1971–2000 between the RCM (C20) and the observed gridded temperatures of each grid point (i, j). To increase the stability of the monthly correction, for each grid point the surrounding eight grid points were additionally considered in order to calculate the average temperature departures (3×3 grid points, the central grid point is the point to be corrected).

In order to avoid discontinuities between the monthly corrections, we calculated a cubic spline that passes through all 12 monthly correction terms (Blümel and Chmielewski, 2011). The correction for the day $t = 1-365$ (366) was the calculated value for the spline on this day [Eq. (24)]:

$$T_{\text{Model,corr.}}(i, j, t) = T_{\text{Model,uncorr.}}(i, j, t) + \text{spline} \left(\frac{\bar{T}_{\text{Observation}}^{1971-2000;\text{mon}}^{3 \times 3} - \bar{T}_{\text{Model,uncorr.}}^{1971-2000;\text{mon}}^{3 \times 3}}{\bar{T}_{\text{Observation}}^{1971-2000;\text{mon}}^{3 \times 3}} \right) (i, j, t) \quad (24)$$

$T_{\text{Model,corr.}}$ is consequently the air temperature after BIAS correction and $T_{\text{Model,uncorr.}}$ the temperature in the RCM without correction.

3.4. Model versions

We will discuss four different model versions. Model **M1** uses Eq. (1) with the new forcing function $R_f(T_i)$ according to Eq. (23) which was extended by the daylength factor. All four parameters (F^* , T_{BF} , t_1 and $EXPO$) were optimized.

The three remaining models make use of Eq. (2) without taking the daylength into consideration. In model **M2**, all three remaining parameters (F^* , T_{BF} and t_1) were fitted. Model **M3** uses the optimal t_1 -value of model **M1** ($t_1 = 6 \text{ DOY} = \text{const.}$) and only F^* and T_{BF} were optimized. Model **M4** is equal to model **M3**, but the optimal value for T_{BF} was not searched in the range -10°C to $+10^\circ\text{C}$. It was now restricted to $0-10^\circ\text{C}$. This latter range is considered to be a physiologically meaningful temperature range. [The negative T_{BF} , which

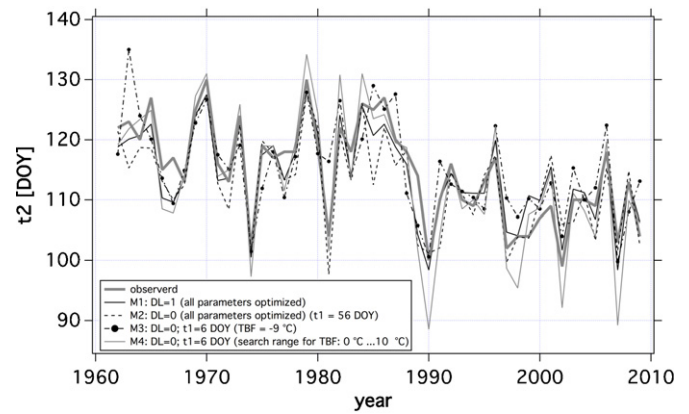


Fig. 6. Observed and calculated dates for the beginning of apple blossom (t_2) 1962–2009, calculated with observed temperatures, and derived from different model versions at a grid point near the city Frankfurt/Main. All model versions were calibrated for the even years in 1962–2009. Shown are all years (even and odd) from 1962 to 2009 [DL = 1: with daylength term, Eq. (23); DL = 0: without a daylength term, Eq. (2)].

occurs as the optimal parameter in model **M3**, must be regarded as a pure fit parameter. As will be shown below, this value gives better results (smaller errors) than model **M4** which uses a physiologically meaningful, positive T_{BF} .]

3.5. Calibration of phenological models

The unknown parameters F^* , T_{BF} and t_1 in the forcing model (1) and (2) [or (1) and (23) with additional unknown parameter $EXPO$] can be determined by minimizing the root mean square (RMSE) error

$$RMSE(\text{opt}) = \left[\frac{1}{N} \sum_{j=1}^N (t_2(\text{pred}, j) - t_2(\text{obs}, j))^2 \right]^{1/2} \quad (25)$$

between predicted $t_2(\text{pred}, j)$ and observed dates $t_2(\text{obs}, j)$ of beginning of blossom, using observed temperatures for as many years N as data are available. We used a version of the ‘simulated annealing’ procedure (Metropolis et al., 1953; Press et al., 1997) for the minimization procedure.

For optimization, the available data from 1962 to 2009 ($N = 48$) was split into two halves. The 24 even years were used for **optimization** [i.e., to minimize the $RMSE(\text{opt})$]. To check the performance of the model in years, which were not used for calibration purposes (**validation**), we calculated the root mean square error $RMSE(\text{ver})$ over the 24 odd years. Odd years are almost independent of the even years used in optimization. Splitting into two disjoint time ranges (1962–1985 and 1986–2009) would have given better statistical independence of the optimization and validation years. But in this case, the intense advance in t_2 which can be observed past 1989 (see Fig. 6) could not enter into the calibration. Hence the determination of the effective future trend would be less reliable.

3.6. Computation of confidence intervals for the model parameter

Most of the model parameters have very large confidence intervals. To illustrate this, we calculated joint confidence intervals for some of these parameters. The calculations used the method from Chapter 18 of Motulsky and Christopoulos (2003) combined with the 300,000 parameter tuples and the related $RMSE(\text{opt})$ which were tested with the Simulated Annealing procedure. The confidence region extends over all parameter values leading to

a RMSE between the minimal RMSE(opt) and the upper limit RMSE(95). RMSE(95) follows from

$$RMSE(95) = RMSE(opt) \left[F_{k, N-k}^{0.95} \frac{k}{N-k} + 1 \right]^{1/2} \quad (26)$$

$F_{k, N-k}^{0.95}$ is the 95%-quantile of the *F*-distribution with $(k, N - k)$ -degrees of freedom. k is the number of optimized parameters, and N is the number of years which were used for optimization.

4. Results

Here, the model performance on a single grid point near the city Frankfurt/Main (8.8°E, 50.2°N, 149 m a.s.l.) will be investigated.

Table 1 shows the optimized model parameters for the four model versions and their search ranges. Also shown are the RMSE values for the optimization and validation years. Model M1 has a physiologically meaningful base temperature $T_{BF} = 1.7^\circ\text{C}$. The starting day $t_1 = 6$ DOY is reasonable, too. However, in model M2, t_1 shows a relatively late starting day (56 DOY) for temperature accumulation, especially if the model will be further used to project the blossoming date. In model M3, the base temperature T_{BF} has very unrealistic low values (-9.0°C), and model M4 shows reasonable values but has a relatively high RMSE; in particular the RMSE(opt) is more than twice as large as in model M1.

The course of t_2 in the optimization/validation period is visualized in Fig. 6. All four model versions, which were optimized with observed temperatures, show an apparent fairly good agreement with the observed values (grey bold line). But an inspection of the RMSE(ver)-column of Table 1 shows that the root mean square error for model M1 is much lower than for all other models without a daylength term. Even if we consider the relatively late t_1 of model M2 as a substitution for a “switch” to terminate ecodormancy, e.g. caused by a critical photoperiod, this sudden start-up of forcing does not perform as well as the continuous weighting with daylength in Eq. (23) and model M1.

Table 2 shows that for current climate conditions nearly all models are able to simulate the average date of the beginning of apple blossom (23–25 April). However, models M3 and M4 fail in the calculation of the extreme blossoming dates. Again model M1 is the only model which exactly calculates the average beginning of apple blossom (24 April) and also has the lowest deviation in the extreme years.

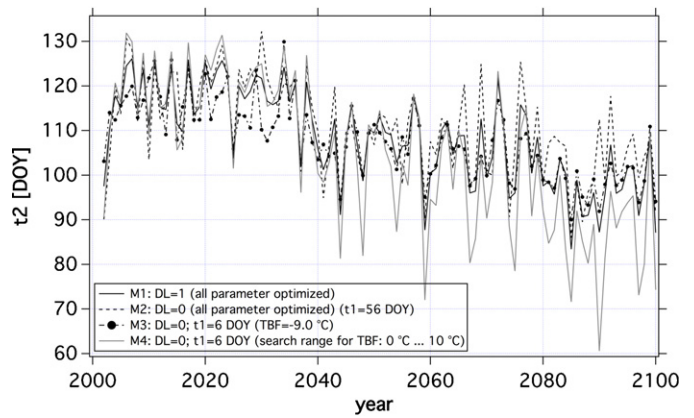


Fig. 7. Beginning of apple blossom (t_2), derived with models M1–M4. Projections with REMO-UBA temperatures (GHG emission scenario A1B) for the grid point near Frankfurt/Main (2002–2100).

The projections of t_2 for the optimized models M1–M4 (Table 1) are shown in Fig. 7. These data were calculated with the temperatures of the REMO-UBA scenario A1B, up to the year 2100 at the selected grid point. The solid black line represents the result of model M1 with the new approach (23). The dashed line (model M2) behaves similarly to the solid black line, but the change of t_2 up to the end of the 21st century (2071–2100 vs. 1971–2000) is approximately 7 days less and amounts to -10.5 days, only (see Table 3). The dot-dashed line (model M3) also shows meaningful behaviour and $\Delta t_2 = -15.4$ days almost equals Δt_2 of model M1. But this result is achieved using a much too low, physiologically unrealistic base temperature $T_{BF} = -9.0^\circ\text{C}$, and the model performed very poorly at validation for the present climate (Table 1). Model M4 (grey line) which has a reasonable base temperature and a useful starting day, shows a very extreme result: The predicted advance in t_2 amounts to -27.1 days and the course displays very strong fluctuations.

In Table 3, in addition to the possible changes Δt_2 , the trends (2011–2100) of t_2 are given for all four models. The numbers in parentheses represent 95%-confidence intervals. The trends (in days per 90 years) are significantly greater than the changes of the 30 year averages in 100 years because the negative slope (advance) in t_2 over time is quite small before 2030 and increases substantially soon afterwards (see Fig. 7).

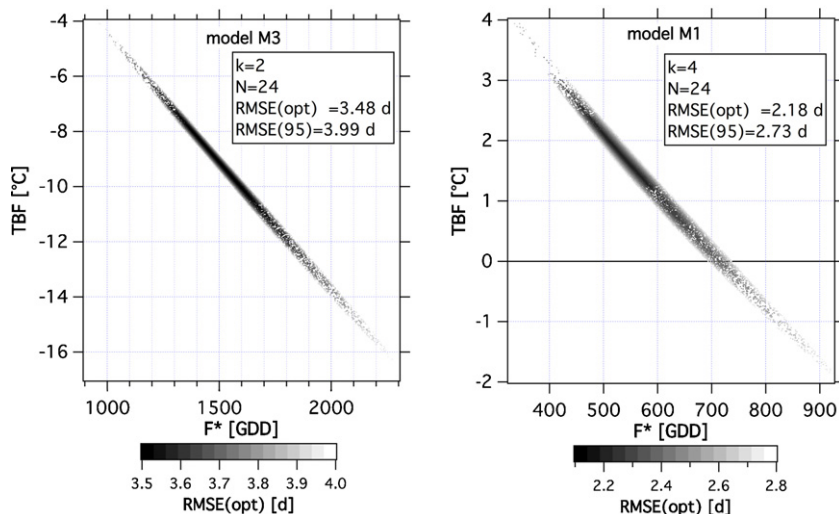


Fig. 8. 95%-confidence interval for T_{BF} and F^* in model M3 (search range for T_{BF} : -40°C to 10°C) (left) and in model M1 (slice for the optimal values $t_1 = 6$ DOY and $EXPO = 1.56$) (right). The “lines” are not identical with the indeterminate range of Fig. 1 because $t_1 > t_s$ in the left figure and the daylength term is used in the right figure.

Table 1

Optimal parameters for the four versions of the Spring-Warming model, derived for apple and the grid point near Frankfurt/Main (at 0.2° resolution).

Model	EXPO [1]	F* [GDD resp. PTU]	T _{BF} [°C]	t ₁ [DOY]	RMSE(opt) [days]	RMSE(ver) [days]
M1	1.56	540.5	1.7	6	2.18	3.99
M2	0.00	220.6	3.5	56	2.59	5.70
M3	0.00	1486.5	-9.0	6	3.48	6.50
M4	0.00	267.9	3.6	6	4.75	5.35
Search range	0–5	100–5000	-10 (0) to 10	1–100	-	-

Table 2Statistical parameters for the observed and calculated dates in the beginning of apple blossom (t₂) with the four versions of the Spring-Warming model, derived for the grid point near Frankfurt/Main (at 0.2° resolution); t₂: mean 1962–2009; Conf95: 95%-confidence interval for t₂; Max: latest date; Min: earliest date for the beginning of apple blossom in the period 1962–2009.

Model	t ₂ [DOY]	Conf95 [days]	Max [days]	Min [days]
Observation	114 (24 April)	2.4	130 (10 May)	99 (9 April)
M1	114 (24 April)	2.2	129 (9 May)	98 (8 April)
M2	113 (23 April)	2.3	128 (8 May)	98 (8 April)
M3	115 (25 April)	2.3	135 (15 May)	100 (10 April)
M4	113 (23 April)	3.2	134 (14 May)	89 (30 March)

Table 3Possible changes Δt₂ (2011–2040, 2041–2070 and 2071–2100 vs. 1971–2000) and trends (2011–2100) in the beginning of apple blossom, derived with the four versions of the Spring-Warming model at the grid point near Frankfurt/Main (at 0.2° resolution) with temperatures from REMO-UBA with GHG emission scenario C20 and A1B. The 95%-confidence interval is shown in parentheses; bold values indicate significant changes of t₂ with *p ≤ 0.05, **p ≤ 0.01, ***p ≤ 0.001.

Model	Δt ₂ (2011–2040 vs. 1971–2000) [days]	Δt ₂ (2041–2070 vs. 1971–2000) [days]	Δt ₂ (2071–2100 vs. 1971–2000) [days]	Trend (2011–2100) [days in 90 a]
M1	0.7 (±4.3)	-11.0 (±4.4****)	-17.1 (±4.8****)	-26.1 (±5.3****)
M2	4.3 (±4.9)	-7.4 (±5.2**)	-10.5 (±5.3****)	-20.8 (±6.2****)
M3	-1.3 (±3.9)	-10.6 (±3.6****)	-15.4 (±3.7****)	-21.1 (±4.4****)
M4	0.7 (±5.8)	-17.7 (±6.5****)	-27.1 (±6.9****)	-40.9 (±8.4****)

Confidence parameters for F* and T_{BF} were calculated using the method described in Section 3.6. All parameter tuples which have a RMSE between RMSE(opt) and RMSE(95) are presented in Fig. 8; for model M3 (left) and model M1 (right). Unfortunately, both confidence intervals are rather wide because of the collinearity of both parameters (i.e., large F* can be compensated by small T_{BF} and vice versa). But the confidence region for F* is about three times wider in model M3 than in model M1. And the range for T_{BF} extends from -15 °C until -5 °C whereas it shrinks to -1 °C until 3 °C in model M1.

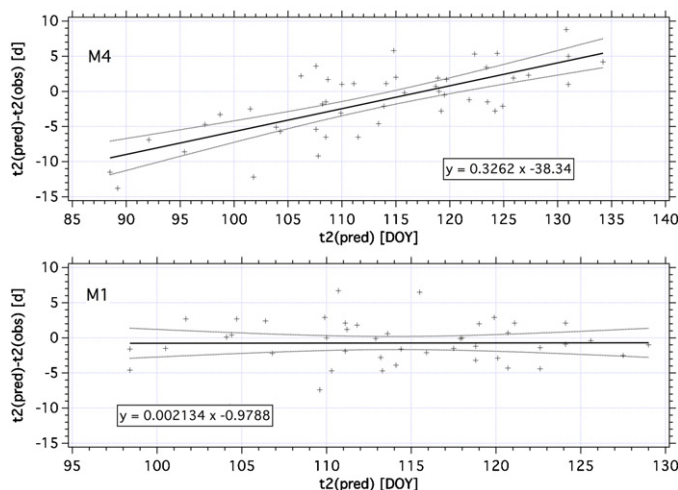
Finally, we will investigate whether the models show any systematic errors. For that reason, the errors in t₂ were plotted against the predicted t₂-values in Fig. 9. This scatterplot of the residuals

(e.g., Wilks, 2006, Chapter 6.2.6) yields to a significant, systematic error (slope of the regression line) of about 33% in model M4 (Fig. 9, upper graph). With the help of Eq. (23) (model M1), this error is reduced to -0.2% (Fig. 9, lower graph). At model M2, the error results in 8.5% and in 17% at model M3. This result strongly emphasizes the use of model M1 for the projection of possible changes in plant phenology.

5. Discussion

Phenological models of type M2 are currently often used to calculate the timing of phenological events. Even the model of García-Mozo et al. (2009a) for determination of the flowering date of olive trees in Spain and Italy, which includes photoperiod as a co-variable in addition to temperature, is of type M2. In their model the photoperiod is used as a “step function” to switch on the forcing accumulation at the date when photoperiod reaches a critical value P₀ which is a new parameter to be optimized. This procedure is equivalent to optimizing t₁ in our model M2 if only a single location or a small region is considered. The same is true for the models with photoperiod limitations given by Migliavacca et al. (2012).

Due to a missing (continuous) daylength term in this model type, the optimal starting date for temperature accumulation is often at the end of February or the beginning or even in the middle of March (Zavalloni et al., 2006; Fisher et al., 2007: 20 March) when the winter season ends and the temperatures are predominantly favourable for bud development. Unfortunately, these models are not suitable for projecting possible shifts in plant development for changed (future) climate conditions, since rising temperatures in January or February are not considered by the models, provided that the endodormancy is still released up to the end of December. For this reason the starting date for temperature accumulation was sometimes fixed at 1 January (Hänninen and Kramer, 2007; Chuine et al., 1999). In this case the optimal base temperature T_{BF} has the tendency to decrease, in order to make t₅ [see Eq. (6) and (19)]

**Fig. 9.** Scatter plot for the residuals as function of the predicted t₂-values for model M4 and M1 for apple at the grid point near Frankfurt/Main.

less than t_1 . Only then, the trend of t_2 with respect to b can be calibrated. A good example for this behaviour is model M3 in Table 1. In model M4, T_{BF} is not allowed to become negative. As a consequence, not only the $RMSE(ver)$ but also the $RMSE(opt)$ adopts large values. Only the introduction of the daylength term offered an acceptable solution to this problem. With that addition, the models were able to consider temperatures as early as in the beginning of the year, assuming that the dormancy is already broken. The daylength limits the influence of temperature on bud development in the beginning of the year, so that the model calculates the plant development for current and probably also for warmer climate conditions more realistically. For this reason, model M1 always showed the best performance in our study. Over and above, the residuals between the simulated and observed values showed no trend, and the very large confidence intervals of T_{BF} and F^* were reduced remarkably.

The improvements by the daylength term were also confirmed by a “regional” phenological model (unpublished). This model used one optimal parameter set for all 81 grid points in 0.2° resolution which cover the federal state of Hessen. The average $RMSE(ver)$ was 1.3 days smaller than in the versions without a daylength term. In the south of Hessen, which is the most intensely cultivated area for fruit trees, model M1 even showed $RMSE(ver)$ values which were up to 5 days lower than in the other model versions.

Even combined chilling-forcing models (Matzneller et al., submitted for publication) are strongly improved by the introduction of a daylength term in the forcing part of the model equations. Without a daylength term, the validation of these models yields strong biases. The end of dormancy is calculated too late and, respectively, the chilling requirement determined by calibration takes on too-high values compared with information given in the literature (e.g., Linkosalo et al., 2006). Hence they cannot be used to project possible shifts in the timing of phenological events until 2100. The chilling part of these combined models will become important under future climate conditions with increasing winter temperatures, since these can cause a delay in the break of dormancy or, at worst, no release at all will be achieved (if the break of dormancy is delayed or advanced additionally depends on the chilling model type and on the chilling requirement of the considered plant species, see Chmielewski et al., submitted for publication). These consequences cannot be described by pure forcing models. With a daylength term, the combined chilling-forcing models can be used for climate change projections until 2100. Matzneller et al. (submitted for publication) showed by means of external validations for tart cherry that the relative reduction in $RMSE(ver)$ was even greater than in Table 1 (30–50%). Moreover, their model was optimized for one location in Germany, but could be applied successfully in Central Europe and at one station in North America.

6. Conclusion

Our study has shown that the original, commonly used phenological forcing models show several systematic shortcomings: If one uses physiologically meaningful values for the starting date of temperature accumulation (t_1) and base temperature (T_{BF}), the models exhibit a built-in trend for the beginning of blossom (t_2) with increasing temperature level (b), which cannot be influenced by the model parameters itself and which is too large in absolute value. As a consequence, large $RMSE$ (e.g., model M4 in Table 1) values emerge.

Implementation of an additional daylength term in the forcing function eliminates all these problems almost entirely, and reduces the $RMSE$ at validation, remarkably. Additionally, this term automatically leads to physiologically meaningful model parameters.

As already mentioned, the physiological influence of daylength on plant development is still controversial (see references in the

Introduction). So, we cannot guarantee that there is indeed a physiological response to daylength for all plants, but the models improved their performance for each of the 9 fruit species which were mentioned in Section 2.3 if a daylength term was considered.

Acknowledgements

This research was funded by the Hessen State Office for Environment and Geology (HLUG) within the research initiative INKLIM-A. We thank the Hessen State Office for Environment and Geology for the awarded grant.

References

- Blümel, K., Chmielewski, F.-M., 2011. Climate change in Hessen—Chances, risks, and costs for fruit growing and viticulture. Annual Report, Hessen State Office for Environment and Geology (HLUG), 82 pp. (in German).
- Caffarra, A., Donnelly, A., 2011. The ecological significance of phenology in four different tree species: effects of light and temperature on bud burst. *Int. J. Biometeorol.* 55, 711–721.
- Chmielewski, F.-M., Blümel, K., Páľešová, I. Climate change and possible shifts of dormancy release for deciduous fruit crops in Germany. *Climate Res.*, submitted for publication.
- Chuine, I., Cour, P., Rousseau, D.D., 1999. Selecting models to predict the timing of flowering of temperate trees: implications for tree phenology modelling. *Plant Cell Environ.* 22, 1–13.
- Chuine, I., Morin, X., Bugmann, H., 2010. Warming, photoperiods, and tree phenology. *Science* 329 (5989), 277–278.
- Fisher, J.L., Richardson, A.D., Mustard, J.F., 2007. Phenology model from surface meteorology does not capture satellite-based greenup estimations. *Glob. Change Biol.* 13, 707–721.
- García-Mozo, H., Orlandi, F., Galán, C., Fornaciari, M., Romano, B., Ruiz, L., Díaz de la Guardia, C., Trigo, M.M., Chuine, I., 2009a. Olive flowering phenology variation between different cultivars in Spain and Italy: modeling analysis. *Theor. Appl. Climatol.* 95, 385–395.
- García-Mozo, H., Galán, C., Belmonte, J., Bermejo, D., Candau, P., Díaz de la Guardia, C., Elvira, B., Gutiérrez, M., Jato, V., Silva, I., Trigo, M.M., Valencia, R., Chuine, I., 2009b. Predicting the start and peak dates of the *Poaceae pollen* season in Spain using process-based models. *Agric. Forest Meteorol.* 149, 256–262.
- Häkkinen, R., Linkosalo, T., Hari, P., 1998. Effects of dormancy and environmental factors on timing of bud burst in *Betula pendula*. *Tree Physiol.* 18 (10), 707–712.
- Hänninen, H., 1995. Effects of climatic change on trees from cool and temperate regions: an ecophysiological approach to modelling of bud burst phenology. *Can. J. Bot.* 73 (2), 183–199.
- Hänninen, H., Kramer, K., 2007. A framework for modelling the annual cycle of trees in boreal and temperate regions. *Silva Fenn.* 41 (1), 167–205.
- Heide, O.M., Presturd, A.K., 2005. Low temperature, but not photoperiod, controls growth cessation and dormancy induction and release in apple and pear. *Tree Physiol.* 25, 109–114.
- Hunter, A.F., Lechowicz, M.J., 1992. Predicting the timing of budburst in temperate trees. *J. Appl. Ecol.* 29, 597–604.
- Jacob, D., Bärting, L., Christensen, O.B., Christensen, J.H., Hagemann, S., Hirschi, M., Kjellström, E., Lenderink, G., Rockel, B., Schär, C., Seneviratne, S.I., Somot, S., van Ulden, A., van den Hurk, B., 2007. An inter-comparison of regional climate models for Europe: design of the experiments and model performance. *Climatic Change* 81 (May (Suppl. 1)), PRUDENCE Special Issue.
- Körner, C., 2006. Significance of temperature in plant life. In: Morrison, J.L.L., Morecroft, M.D. (Eds.), *Plant Growth and Climate Change*. Blackwell, Oxford, pp. 48–69.
- Körner, C., Basler, D., 2010. Phenology under global warming. *Science* 327 (5972), 1461–1462.
- Körner, C., Basler, D., 2011. Temperature and photoperiodic control of spring bud burst in temperate forest trees at rising spring temperatures. *Geophys. Res. Abstr.* 13, EGU2011-10159, EGU General Assembly 2011.
- Linkosalo, T., Häkkinen, R., Hänninen, H., 2006. Models of the spring phenology of boreal and temperate trees: is there something missing? *Tree Physiol.* 26 (9), 1165–1172.
- Linkosalo, T., Lappalainen, H.K., Hari, P., 2008. A comparison of phenological models of leaf bud burst and flowering of boreal trees using independent observations. *Tree Physiol.* 28, 1873–1882.
- Matzneller, P., Blümel, K., Chmielewski, F.-M. Chilling and forcing models improved by a daylength-term to predict the beginning of sour cherry blossom. *Agric. For. Meteorol.*, submitted for publication.
- Metropolis, N., Rosenbluth, A.W., Rosenbluth, M.N., Teller, A.H., Teller, E., 1953. Equation of state calculations by fast computing machines. *J. Chem. Phys.* 21 (6), 1087–1092.
- Migliavacca, M., Sonntag, O., Keenan, T.F., Cescatti, A., O’Keefe, J., Richardson, A.D., 2012. On the uncertainty of phenological responses to climate change and its implication for terrestrial biosphere models. *Biogeosci. Discuss.* 9, 879–926.

- Morin, X., Lechowicz, M.J., Augspurger, C., O'Keefe, J., Viner, D., Chuine, I., 2009. Leaf phenology in 22 North American tree species during the 21st century. *Glob. Change Biol.* 15, 961–975.
- Motulsky, H., Christopoulos, A., 2003. *Fitting Models to Biological Data Using Linear and Nonlinear Regression: A Practical Guide to Curve Fitting*, 1st ed. Oxford University Press, USA, 351 pp.
- Muneer, T., 2004. *Solar Radiation and Daylight Models*, 2nd ed.: For the Energy Efficient Design of Buildings. Elsevier Butterworth-Heinemann Publications, 341 pp. ISBN-10: 0750659742.
- Press, W.H., Teukolsky, S.A., Vetterling, W.T., Flannery, B.P., 1997. *Numerical Recipes in Fortran 77. The Art of Scientific Computing*, 2nd ed. Cambridge University Press, 994 pp.
- Roeckner, E., Arpe, K., Bengtsson, L., Christoph, M., Claussen, M., Duemenil, L., Esch, M., Giorgetta, M., Schlese, U., Schulzweida, U., 1996. The atmospheric general circulation model ECHAM4: model description and simulation of present-day climate. Report Nr. 218, Max-Planck-Institut für Meteorologie, Hamburg.
- Roeckner, E., Bäuml, G., Bonaventura, L., Brokopf, R., Esch, M., Giorgetta, M., Hagemann, I., Kirchner, S., Kornbluh, L., Manzini, E., Rhodin, A., Schlese, U., Schulzweida, U., Tompkins, A., 2003. The atmospheric general circulation model ECHAM5: Part I: Model description. Report Nr. 349, Max Planck Institut für Meteorologie, Hamburg, 127 pp.
- Schaber, J., Badeck, F.-W., 2002. Evaluation of methods for the combination of phenological time series and outlier detection. *Tree Physiol.* 22 (14), 973–982.
- Schaber, J., Badeck, F.-W., 2003. Physiology-based phenology models for forest tree species in Germany. *Int. J. Biometeorol.* 47, 193–201.
- Vitasse, Y., Francois, C., Delpierre, N., Dufrene, E., Kremer, A., Chuine, I., Delzon, S., 2011. Assessing the effects of climate change on the phenology of European temperate trees. *Agric. Forest Meteorol.* 151, 969–980.
- Wackernagel, H., 1998. *Multivariate Geostatistics. An Introduction with Applications*. Springer-Verlag, Berlin/Heidelberg/New York, 291 pp.
- Wilks, D.S., 2006. *Statistical Methods in the Atmospheric Sciences*, 2nd ed. Elsevier, Academic Press, 627 pp.
- Zavalloni, C., Andersen, J.A., Flore, J.A., 2006. Phenological models of flower bud stages and fruit growth of 'Montmorency' sour cherry based on growing degree-days accumulation. *J. Amer. Soc. Hort. Sci.* 131, 601–607.